Nanostructured Surfaces Frustrate Polymer Semiconductor Molecular Orientation

Danvers E. Johnston,[†] Kevin G. Yager,[†] Htay Hlaing,[‡,§] Xinhui Lu,[‡] Benjamin M. Ocko,[‡] and Charles T. Black[†,*]

[†]Center for Functional Nanomaterials, Brookhaven National Laboratory, Upton, New York 11973, United States, [‡]Condensed Matter Physics & Materials Science Department, Brookhaven National Laboratory, Upton, New York 11973, United States, and [§]Department of Physics & Astronomy, Stony Brook University, Stony Brook, New York 11790, United States

ABSTRACT Nanostructured grating surfaces with groove widths less than 200 nm impose boundary conditions that frustrate the natural molecular orientational ordering within thin films of blended polymer semiconductor poly(3-hexlythiophene) and phenyl-C_{61}-butyric acid methyl ester, as revealed by grazing incidence X-ray scattering measurements. Polymer interactions with the grating sidewall strongly inhibit the polymer lamellar alignment parallel to the substrate typically found in planar films, in favor of alignment perpendicular to this orientation, resulting in a preferred equilibrium molecular configuration difficult to achieve by other means. Grating surfaces reduce the relative population of the parallel orientation from 30% to less than 5% in a 400 nm thick film. Analysis of in-plane X-ray scattering with respect to grating orientation shows polymer backbones highly oriented to within 10 degrees of parallel to the groove direction.

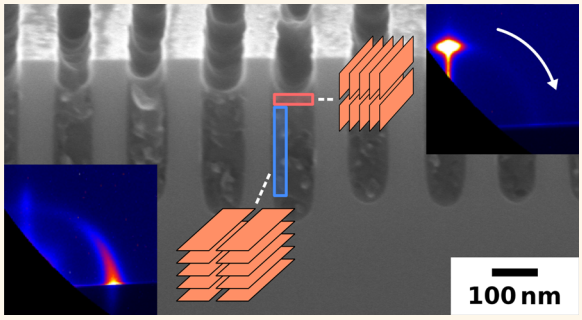

KEYWORDS: organic semiconductor · X-ray scattering · conjugated polymer · organic solar cell · crystalline polymer

Conjugated polymers have found application in electronic devices such as field-effect transistors,[1,2] light-emitting diodes,[3] and solar cells.[4] The material's molecular arrangement dramatically influences its electronic and optical properties. For example, the electronic mobility of regioregular poly(3-hexlythiophene) (P3HT) can vary significantly with molecular weight and degree of molecular crystallization and orientation.[5−7] The electrical conductivity[2,8] and light absorbance[9] of crystalline P3HT are directionally anisotropic, with charge transfer along polymer backbones and between π-stacked chains easier than across insulating side-chains.

Thin-film blends of highly regioregular P3HT and phenyl-C_{61}-butyric acid methyl ester (PCBM) have been widely studied for semiconductor photoactive layers in organic bulk heterojunction solar cells. In this work, we examine the crystalline P3HT structure within P3HT:PCBM blends confined to one-dimensional (1D) grooves with widths <200 nm and find that competing horizontally and vertically oriented interfaces frustrate the natural P3HT molecule orientational ordering exhibited on flat surfaces.

RESULTS AND DISCUSSION

Thin films of a 50:50 wt % P3HT:PCBM composite cast from a slow-evaporating solvent (chlorobenzene) (*e.g.*, 240 nm thickness, Figure 1a) include a crystalline P3HT population with a strong degree of lamellar alignment parallel to the substrate,[1,8,10,11] as evidenced by the 2D grazing incidence wide-angle X-ray scattering pattern (GIWAXS) showing three equally spaced peaks in the out-of-plane direction, located at q_z = 0.39, 0.77, and 1.15 Å^{-1} (Figure 1b). In our discussion, we use the conventional P3HT crystallographic notation, with this lamellar direction defined as <100>, the $\pi-\pi$ stacking direction as <010>, and the polymer backbone direction as <001>.[12] A line-cut along the out-of-plane scattering direction (Supporting Information) shows that these peaks are consistent with a 1.60 nm spacing between stacked P3HT lamellae, in agreement with previous observations.[1,2,11,12] The scattering

* Address correspondence to ctblack@bnl.gov.

Received for review June 28, 2013 and accepted December 16, 2013.

Published online December 16, 2013
10.1021/nn4060539

© 2013 American Chemical Society

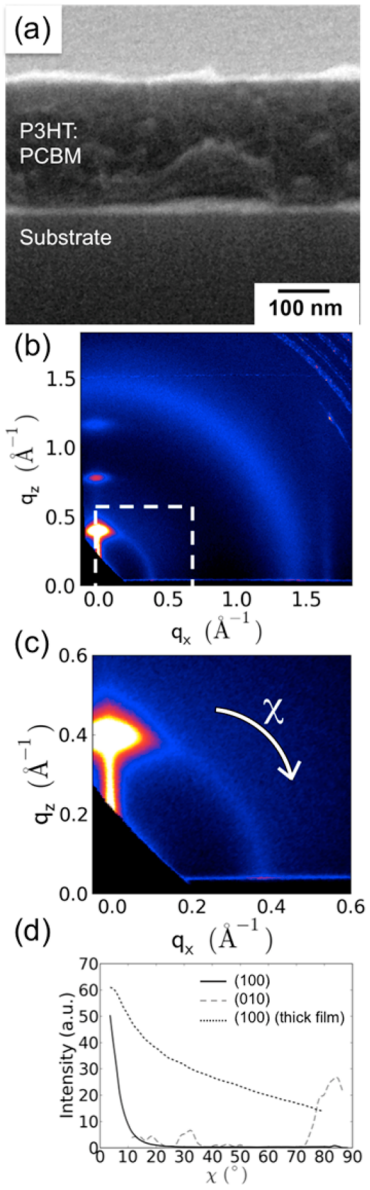

Figure 1. (a) 70 degree angle SEM cross-section of a P3HT:PCBM film. (b) 2D GIWAXS pattern from a P3HT:PCBM thin film on a planar substrate. (c) Magnified 2D GIWAXS pattern (area bounded by white box in (b)), emphasizing the (100) scattering peak. (d) Angular cuts of scattering intensity along arc of constant $|q|$ corresponding to P3HT (100) lamellar scattering peak in (solid line) spin-cast 200 nm thick film, and (dotted line) drop-cast 4.4 μm thick film. Dashed line shows an angular cut of scattering intensity along an arc of constant $|q|$ corresponding to P3HT (010) $\pi-\pi$ stacking in a spin-cast 200 nm thick film.

from a planar film (see Figure 1c) provides a baseline for understanding the structural changes induced by the nanostructured grooves. The scattering intensity as a function of polar angle (χ) with respect to the surface normal at $|q| = 0.39$ Å^{-1}, corresponding to the q-vector of the (100) planes, is a measure of the P3HT orientation. The χ scattering profile shows that the lamellar alignment is predominantly parallel to the substrate ($\chi \sim 0°$) (Figure 1d, solid line). A Scherer peak width analysis of the radial scattering profile, including

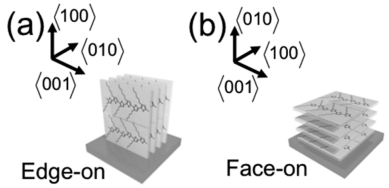

Figure 2. Schematic (a) edge-on and (b) face-on P3HT orientations.

GIWAXS instrumental broadening,[13] reveals a P3HT coherence length of ξ = 21 nm along the lamellar stacking direction, similar to previous findings.[1] A weaker, vertical streak of scattering at q_x = 1.64 Å^{-1} (Figure 1b), corresponding to a distance of 0.38 nm, is consistent with (010) $\pi-\pi$ stacking, oriented within the substrate plane, at $\chi \sim 90°$ (Figure 1d, dotted line). These observations together imply a significant fraction of the ordered P3HT population within the P3HT:PCBM blend is oriented "edge-on" (shown schematically in Figure 2a). A 90° reoriented P3HT lattice with backbone oriented in the surface plane is termed "face-on" (Figure 2b).[1,8,10,11] The broad ring at $|q|$ = 1.37 Å^{-1} (0.46 nm) is scattering from phase separated, noncrystalline PCBM. In this work we focus exclusively on the effect of confinement on the P3HT phase within blended P3HT:PCBM, as we have not observed any measurable grating-induced change in scattering from PCBM.

Thin films of the P3HT:PCBM blend exhibit a strong preference for the edge-on orientation, likely arising from ordering at both the substrate and film−air interfaces (parallel to each other). In particular, the P3HT side-chains preferentially wet these interfaces, as this configuration is driven by the lower interfacial energy of terminal methyl groups.[14,15] For example, from analysis of a similar angular line-cut of the (100) scattering peak of a drop-cast P3HT:PCBM film, >10 times thicker (t = 4.4 μm) (Figure 1d, dashed line), we estimate that ~20−30% of the crystalline P3HT population is oriented in the edge-on configuration. This is a significantly higher fraction of the film volume than would be the case if the orientational order extended only a distance ~ξ away from substrate and air interfaces (which would contain only (2 × 21 nm)/4400 nm ≈ 1%). The increase in scattering intensity across all angles is due to crystalline P3HT without a preferred orientation (*i.e.*, isotropic), presumably in the film interior.[15]

We present X-ray scattering measurements of the P3HT molecular morphology when confined to grooves with widths between 50 nm < w < 170 nm and depths between 150 nm < d < 520 nm (Table 1). We fabricated silicon substrates into parallel arrays of 1D grooves, with nanometer-scale width (w) and depth (d) defined using electron-beam lithography and reactive-ion etching.[16] We dehydrate the Si grating substrates by baking at 250 °C (10 m on a hot plate, in Ar) prior to spin-casting the P3HT:PCBM blend.

TABLE 1. Nanostructured Groove Dimensions and Polymer Film Thicknesses Used in Experiments[a]

Nominal groove width (nm)	Average groove width (w) (nm) 	Average groove depth (d) (nm) 	Average film thickness (t) (nm) 
45	47 ± 2	143 ± 3	129 ± 6
80	87 ± 5	324 ± 13	262 ± 15
100	113 ± 11	455 ± 18	387 ± 37
140	138 ± 12	490 ± 12	408 ± 36
160	160 ± 10	513 ± 4	429 ± 10
180	175 ± 7	523 ± 6	460 ± 14

[a] Nominal groove widths for nanostructured grating surfaces, and measured average groove width (w), depth (d), and P3HT:PCBM film thickness (t). We measured average values from SEM cross sections. Uncertainties represent one standard deviation calculated from a minimum of 5 measurements.

We confirmed template filling and measured the thickness within the grooves (t) using scanning electron microscopy. The reported thickness values are average measurements from a minimum of 5 grooves, with uncertainty corresponding to one standard deviation on this mean. We removed all organic material from the template's top surface, as well as from the planar substrate surrounding the ~mm^2 patterned grating region, in order to avoid collecting signal from X-ray scattering of unconfined material (Supporting Information).

The GIWAXS pattern of a t = 460 nm thick P3HT:PCBM film confined within grooves with average width w = 175 nm and depth d = 520 nm (Figure 3a) shows clear differences in the P3HT (100) lamellar stacking peak (Figures 3b,c), compared to that from a planar P3HT:PCBM film (Figure 1c,d). Here, we maintained the incident X-ray beam parallel to the long-axis of the gratings. Confinement within the grating changes the lamellar orientation, as evidenced by significantly increased scattering intensity at $\chi \sim 90°$ and consistent with P3HT lamellae oriented parallel to the grating's sidewall (Figure 3b, and solid line, Figure 3c). Concomitantly there is a decrease in scattering at $\chi \sim 0°$ and an increase in scattering from isotropically oriented P3HT (appearing as a ring at constant $|q|$ in Figure 3b and as a constant scattering intensity across all angles in Figure 3c, solid line). In further support of the grating-induced reorientation, the (010) scattering intensity from P3HT $\pi-\pi$ stacking is now predominately at $\chi \sim 0°$ (Figure 3c, dotted line). These changes are consistent with an increase in the P3HT face-on population. We do not observe any change in the P3HT molecular arrangement when blend samples are measured at 200 °C (near the P3HT melting point), and also upon recooling to room temperature (Supporting Information). We have also measured similarly invariant orientations in films of pure P3HT in grating grooves, both at room temperature and at 200 °C, as well as infiltrated into gratings at a temperature (230 °C) above the P3HT melting point and then slowly cooled. Because of the invariance with temperature, we believe this represents a thermodynamically stable configuration, rather than a kinetically trapped state such as observed when casting films of P3HT:PCBM from a fast-evaporating solvent.[12]

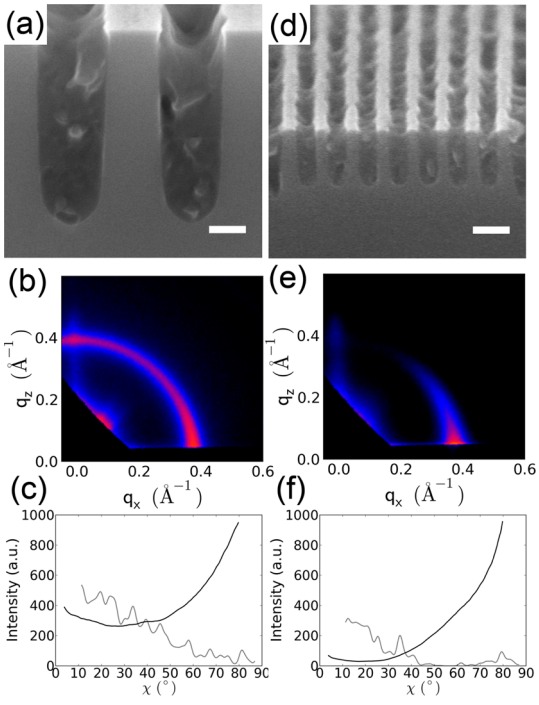

Figure 3. (a,d) 70 degree angle SEM cross-sectional images of silicon gratings with (a) 175 and (d) 47 nm average groove widths, filled with P3HT:PCBM. Scale bar denotes 100 nm. (b,e) Corresponding 2D GIWAXS patterns showing P3HT (100) scattering peak orientation. (c,f) Corresponding angular cuts of scattering intensity showing the distributions of (solid lines) P3HT 100 lamellar scattering peaks, and (dashed line) scattering from (010) $\pi-\pi$ stacking. X-ray beam is parallel to the grating long-axis direction (φ = 0).

Decreasing the confining groove width (w) increases the relative P3HT population with face-on orientation. The smallest average groove width used in this study (w = 47 nm) (Figure 3d) approaches the length-scale of the P3HT crystalline domains (~21 nm) so that most P3HT lies within one correlation length of a groove wall. A quantitative measure of the orientation is provided by the χ scans (Figures 3e,f). The much stronger (100) scattering intensity at $\chi = 90°$, compared to χ = 0°, especially in the 47 nm grooves, strongly supports a preferred lamellar alignment parallel to the groove sidewalls. This arrangement is also supported by the $\pi-\pi$ stacking peak, which is preferentially aligned along the substrate-normal (Figure 3f, dotted line), and azimuthal X-ray scans (discussed below). This is consistent with a face-on molecular orientation that is 90° rotated compared with the orientation found for the planar film. The P3HT lamellar orientation and backbone alignment within the grooves are similar to that measured in pure P3HT films nanoimprinted with similar dimensions[14] and confined within grating channels with ~50 nm width,[16] but contrasts with a study suggesting a significant degree of vertical backbone alignment in pure P3HT films imprinted with deeper grooves.[17,18] Optical measurements of P3HT confined within cylindrical channels having sub-100 nm diameters show a substantial reduction in absorption anisotropy compared to planar P3HT films, consistent with a change in molecular packing orientation,[19] and X-ray measurements show suppression of the edge-on orientation without the significant face-on orientation observed in gratings.[20,21] The present study systematically measures the effect of varying groove width and provides the most direct evidence to date on the effects of confinement on the orientation and alignment of P3HT:PCBM blends.

We analyze the influence of the nanostructured gratings on the relative populations of edge-on, face-on, and isotropically oriented P3HT through quantitative analysis of the angular (χ) distribution of the (100) lamellar peak scattering intensity. Because our measurements exclude the presence of significant vertical alignment of P3HT backbones (discussed further below), the configuration where lamellae are parallel to the vertical sidewalls must necessarily correspond to face-on. For ease of analysis, we have employed a geometric construct (Figure 4a) to determine the fractional populations in each sample. Isotropically oriented P3HT produces a constant scattering intensity across all angles (gray region in Figure 4a). We attribute excess scattering intensity at smaller χ to P3HT oriented edge-on (red region in Figure 4a), and excess scattering intensity at larger χ as due to P3HT oriented face-on (blue region in Figure 4a). Decreasing the groove width (w) increases the fractional P3HT population having face-on orientation, at the expense of edge-on (Figure 4b). For the smallest w in this study

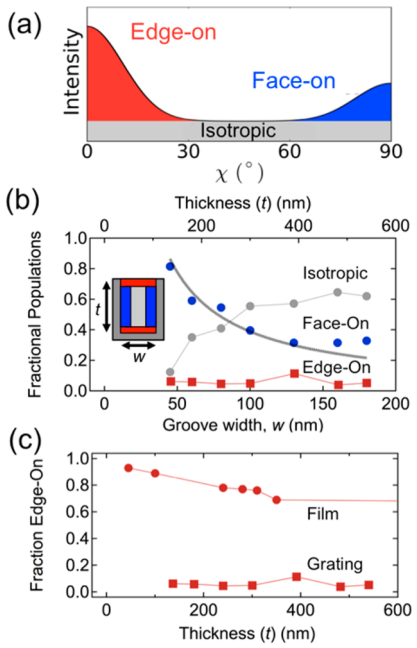

Figure 4. (a) Schematic angular cut of P3HT (100) peak scattering intensity, with contributions from (red) edge-on, (blue) face-on, and (gray) isotropically oriented P3HT. (b) Fractional populations of (red squares) edge-on, (blue dots) face-on, and (gray dots) isotropically oriented P3HT *versus* confining groove width, w. Thick gray line is a plot of ~2ξ/w (ξ = 21 nm) for w > 42 nm. Inset: Model showing locations of (red) edge-on, (blue) face-on, and (gray) isotropic P3HT populations within confining grooves. (c) Fractional P3HT edge-on populations *versus* thickness for (dots) planar P3HT:PCBM films and (squares) films confined to grooves.

(47 nm), we estimate >80% of the crystallized P3HT is oriented face-on, as a consequence of surface interactions with the vertical grating sidewalls. Our data show that even grooves as large as w = 175 nm orient ~30% of the crystalline P3HT population as face-on, with an additional >60% isotropically oriented—a consequence of our fabrication scheme, in which groove height-to-width aspect ratios emphasize sidewall interactions over the top and bottom interfaces. The P3HT face-on population decreases similarly with increasing grating width for samples heated to 200 °C (Supporting Information).

Our data are quantitatively described by a simplified geometric model that assumes P3HT located within a distance ξ of the two vertical walls will orient face-on, P3HT located within a distance ξ from film top and bottom surfaces orients edge-on, and the remaining film volume has an isotropic orientation (Figure 4b, inset). This model predicts a fractional face-on population of ~2ξ/w (for w > 2ξ), in good agreement with the observed decrease in P3HT face-on population with increasing groove width (w). The thick gray line in Figure 4b plots ~2ξ/w *versus* w and accurately describes the face-on population (blue circles) (with ξ = 21 nm calculated from a Scherer analysis of the P3HT (100) lamellar peak width). This supports the

conclusion that all interfaces (air, substrate, and grating sidewalls) have a similar effect of directing P3HT orientation over an intrinsic coherence length, ξ.

Nanostructured grating surfaces frustrate the P3HT lamellar alignment parallel to the surface that occurs naturally in planar P3HT:PCBM films, most clearly evidenced by comparing the fractional populations of edge-on P3HT in blend films of similar thickness (t) applied to planar and grating substrates (Figure 4c). In a P3HT:PCBM film on a planar substrate, the air and substrate interfaces both induce an edge-on P3HT orientation, and together these cause the entire film to be predominantly edge-on even at thicknesses substantially exceeding the average P3HT grain size ($\xi \sim 21$ nm). For example, the crystalline regions of planar P3HT:PCBM films with ~100 nm thickness are >60% edge-on oriented (Figure 4c). Introducing competing interfaces driving a face-on orientation disrupts this synergistic ordering. The four confining interfaces of the grating groove each order the material over a correlation length (~20 nm), but preferred orientational order within the bulk is frustrated. Introducing a grating with average groove width $w = 47$ nm reduces the edge-on population in ~100 nm thick P3HT:PCBM to less than 5% (from >60%, Figure 4c). While ~30% of the P3HT in a ~400 nm thick planar blend film remains oriented edge-on, confining grooves with $w = 140$ nm suppress the edge-on orientation to ~5% of the total population. Because charge transport through stacked P3HT lamellae is poor,[2,8] it is likely that reducing the population with edge-on orientation will significantly improve the out-of-plane P3HT charge mobility.[16,17,19,20]

We obtain complete three-dimensional information about the P3HT molecular stacking orientation by rotating samples along the in-plane azimuthal angle (φ) with respect to the incident X-ray beam. Azimuthal rotation of the grating axis away from the incoming X-ray beam ($\varphi = 0°$, Figure 5a) strongly decreases the (100) scattering close to $\chi = 90°$, consistent with P3HT lamellae being parallel to the grating's vertical side walls (Figure 5a–d show scattering intensity from the (100) peak for increasing φ). For $\varphi > 45°$, the GIWAXS pattern shows no contribution from P3HT lamellae at $\chi = 90°$ (Figure 5d). In contrast, scattering from P3HT lamellae aligned parallel to the substrate ($\chi = 0°$) is independent of φ, as expected (Figure 5a–d). The presence of excess scattering intensity at $\chi = 0°$ for the P3HT (010) π–π stacking peak for all φ, combined with the strong φ-dependence of the (100) lamellar scattering peak, is only consistent with a face-on orientation with P3HT polymer backbones oriented along the grating axis direction. By itself, the P3HT (100) peak intensity at $\varphi = 0°$ and $\chi = 90°$ could be ascribed to either a face-on or vertical orientation; however, this is not supported by the full data set. We exclude a vertical P3HT backbone orientation *without* lamellar orientation on the basis of the strong

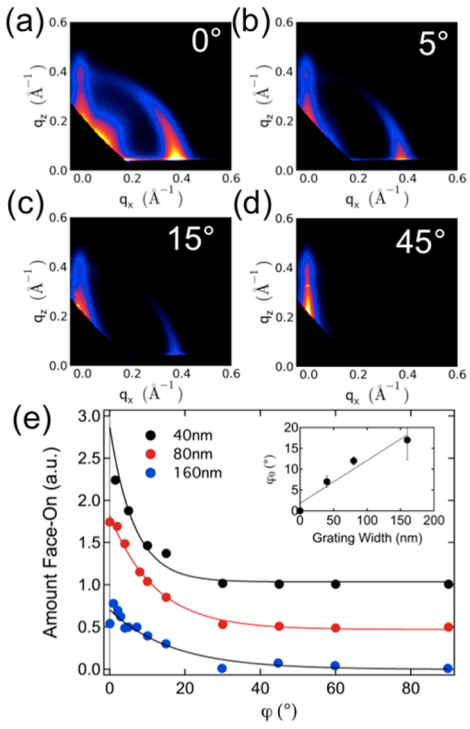

Figure 5. (a–d) 2D GIWAXS intensity plots for a P3HT:PCBM film confined within grooves with average width of 47 nm, for azimuthal angles (φ) of 0, 5, 15, and 45 degrees. (e) Plot of normalized in-plane P3HT 100 lamellar peak scattering intensity *versus* azimuthal angle for (black) 47, (red) 87, and (blue) 175 nm average groove widths. Red and black data are offset from the horizontal axis for clarity. Solid lines are exponential fits to the data. (inset) Characteristic decay angle (φ_0) *versus* groove width (w). Solid line is a linear fit to the data.

φ-dependence of the (100) peak. A vertical orientation *with* lamellae oriented along the groove direction is also excluded because of the absence of any strong (010) peak oriented at $\varphi = 90°$. Nevertheless, the P3HT population we identify as isotropic includes all possible orientations, including a small vertical-like fraction.

Analysis of the decrease in the integrated first-order P3HT in-plane lamellar peak scattering intensity *versus* azimuthal scattering angle (φ) provides a measure of the degree of P3HT backbone orientation along the grating axis (Figure 5e). For the three average confining groove widths shown ($w = 47$, 87, and 175 nm), the in-plane scattering intensity decreases rapidly as φ increases away from parallel to the grating axis. In all cases, the decay is reasonably well described by an exponential expression $\sim \exp(-\varphi/\varphi_0)$, with φ_0 a characteristic angular decay value (solid lines in Figure 5e). The P3HT backbones are closely aligned to grating walls, to within $\varphi_0 = 7°$, for the narrowest confining grooves ($w = 47$ nm). Wider gratings offer less confinement, with correspondingly broadened P3HT backbone angular distribution; however, even $w = 175$ nm groove widths align polymer chains to within $\varphi_0 = 16°$ of the grating axis. One of several possible physical explanations is consistent with previous studies of P3HT structure,

which have shown that P3HT backbones can aggregate into elongated needle-like structures.[6,22−24] A needle of length l confined within the grooves would align within $\sin\varphi_0 \sim \varphi_0 \sim w/l$, for $l \gg w$. From the slope of the best fit to φ_0 *versus* w (Figure 5e, inset), we estimate $l \sim w/\varphi_0 \sim 590$ nm, roughly consistent with previous observations of P3HT molecular structure by atomic force microscopy[5,6,22] and electron microscopy.[22,23]

CONCLUSIONS

Confining blended P3HT:PCBM within nanostructured grooves induces a 90° P3HT backbone reorientation near the grating sidewalls, which frustrates the strong tendency of P3HT molecules to orient edge-on relative to substrate and air interfaces in planar thin films. Nanoconfinement thus enables one to either select a particular orientational state, or else emphasize the isotropic state caused by competing wall interactions.

METHODS

Grazing-incidence wide-angle X-ray scattering (GIWAXS) measurements were performed at the undulator-based X9 endstation at the National Synchrotron Light Source (NSLS), Brookhaven National Laboratory. Two-dimensional scattering images were acquired using an area detector, positioned 217 mm from the sample, and using an X-ray wavelength of 0.10332 nm (photon energy of 12.00 keV). Data conversion to q-space was accomplished by measuring a standard sample with known scattering features (Silver Behenate), and accounting for detector position and tilt angle. The incident beam was collimated using slits and focused onto the sample position using a KB mirror system; the beam size at the sample position was approximately 100 μm horizontal width and 50 μm vertical width. Measurements were performed at a variety of incident angles (0.07°, 0.10°, 0.15°, 0.20°, 0.30°); all measurements above the critical angle had similar features. The results presented in the manuscript used the data at 0.20°, which is well above the critical angle for any of the films studied, and is thus representative of the entire film.

We computed the P3HT correlation length from the scattering peak width using a Debye−Scherer analysis, accounting for instrumental broadening of the peak and intersection of the scattering with the detector geometry.[13]

In order to quantify the orientation distribution of ordered P3HT, we integrated the 100 lamellar peak along the arc at $|q| = 0.38$ Å^{-1} at each angle (χ) with respect to the q_z axis.[16,20] The background at each χ was subtracted by measuring the average intensity just outside the peak. This method removes any diffuse scattering contribution. The full peak width was integrated at each χ, in order to account for variation in peak width between samples and with angle for a given sample. The χ scale was corrected to account for the intersection of the Ewald sphere with reciprocal space.[25] To convert from detector intensity to the amount of material within a particular orientation-population, one must compute the integrated intensity throughout all of reciprocal space (and not merely the slice of reciprocal space measured by the detector plane). In our case, we intend to make a cross-comparison between planar samples, which are in-plane powders, and grating-confined samples, which are anisotropic in-plane. In an in-plane powder, the radial symmetry (about the q_z axis) allows us to compute the integrated scattering by multiplying the detector peak intensity by $\sin(\chi)$. This geometric correction factor is not applicable to the grating samples. In this case one could instead compute integrated intensity by reconstructing the full three-dimensional reciprocal space of the sample. As we demonstrate, the P3HT 100 peak is highly concentrated near $\varphi = 0°$ (grating aligned with X-ray beam). Thus, for these samples the direct detector image at $\varphi = 0°$ is used as a reasonable approximation for the orientation distribution of the material. We note that we do not cross-compare intensities between these two modes of data analysis: instead we compute *relative* populations in each case, and only compare those.

Fabrication of grooved templates began with patterning a p-doped Si wafer (1−12 Ω-cm) by electron beam lithography using a JEOL JBX6300-FS (100 kV, 220 μC/cm^2, 150 pA). ZEP-520A resist (Zeon Corporation) was spin coated to a thickness of 50 nm for use as the resist and etch mask. Exposed resist was developed in hexyl-acetate (90 s), followed by isopropanol (90 s) and rinse in deionized water (90 s). Pattern transfer to the Si was performed by inductively coupled reactive ion etching using an Oxford Instruments Plasmalab 100 (40 sccm SF_6, 18 sccm O_2, 12 mTorr, −100 °C, ICP 800 W, RF 40 W for 3 s followed by 15 W for 20 s). Residual resist was removed using a March plasma etch tool (O_2, 100 mTorr, RF power 20 W for 1 min). Substrates were dehydrated on a hot plate for 10 min at 250 °C. A solution of 2.5% or 5% by weight (depending on desired film thickness) 50:50 P3HT (Rieke Metals, Inc., M_w = 50−70K, regioregularity 91−94%): PCBM (American Dye Source) in anhydrous chlorobenzene (Sigma-Aldrich Co.) was prepared in the glovebox and deposited by spin coating at 1000 rpm for 1 min. Excess blend material was removed by sliding a razor blade across the film with the blade pressed firmly in contact with the unetched polished Si surface. We confirmed that the physical process of removing excess material from the grating top surface did not change the molecular orientation of P3HT within grating grooves by comparing GIWAXS data taken from samples of each type (Supporting Information).

Conflict of Interest: The authors declare no competing financial interest.

Acknowledgment. This research is supported by the U.S. Department of Energy, Basic Energy Sciences, at the Center for Functional Nanomaterials (D.J., K.Y., and C.B.) and the Materials Sciences and Engineering Division (H.H., X.L., and B.O.) (Contract No. DE-AC02-98CH10886). This work was partially supported by the Energy Laboratory Research and Development Initiative at Brookhaven National Laboratory.

Supporting Information Available: A line cut of X-ray scattering intensity along q_z from a planar film of P3HT:PCBM, a 2D GIWAXS pattern from a P3HT:PCBM thin film confined within ~50 nm grooves without removing residual organic layer from the top surface, and a 2D GIWAXS pattern from a P3HT:PCBM thin film confined within ~50 nm grooves after annealing at 150 °C. SEM image of a grating with 80 nm grooves filled with P3HT:PCBM and a residual organic layer on top, with corresponding 2D GIWAXS patterns of this sample as-cast, heated to 200 °C, and recooled to room temperature, together with analysis of the P3HT face-on populations under these three conditions in gratings with different groove widths. SEM image of a grating with 80 nm grooves filled with pure P3HT and a residual organic layer on top, with corresponding 2D GIWAXS patterns of this sample as-cast, heated to 200 °C, and recooled to room temperature, together with analysis of the P3HT face-on populations under these three conditions in gratings with different groove widths. A 2D GIWAXS pattern for a pure P3HT film melt-infiltrated at 230 °C into a grating with 45 nm groove widths and slowly cooled to room temperature. These materials are available free of charge *via* the Internet at http://pubs.acs.org.

REFERENCES AND NOTES

1. Kline, R.; McGehee, M.; Toney, M. Highly Oriented Crystals at the Buried Interface in Polythiophene Thin-Film Transistors. *Nat. Mater.* **2006**, *5*, 222–228.

2. Sirringhaus, H.; Brown, P.; Friend, R.; Nielsen, M.; Bechgaard, K.; Langeveld-Voss, B.; Spiering, A.; Janssen, R.; Meijer, E.; Herwig, P.; *et al.* Two-Dimensional Charge Transport in Self-Organized, High-Mobility Conjugated Polymers. *Nature* **1999**, *401*, 685–688.
3. Sirringhaus, H.; Tessler, N.; Friend, R. Integrated Optoelectronic Devices Based on Conjugated Polymers. *Science* **1998**, *280*, 1741–1744.
4. Yu, G.; Gao, J.; Hummelen, J.; Wudl, F.; Heeger, A. Polymer Photovoltaic Cells—Enhanced Efficiencies Via a Network of Internal Donor-Acceptor Heterojunctions. *Science* **1995**, *270*, 1789–1791.
5. Kline, R. J.; McGehee, M. D.; Kadnikova, E. N.; Liu, J.; Fréchet, J. M. J. Controlling the Field-Effect Mobility of Regioregular Polythiophene by Changing the Molecular Weight. *Adv. Mater. (Weinheim, Ger.)* **2003**, *15*, 1519–1522.
6. Kline, R. J.; McGehee, M. D.; Kadnikova, E. N.; Liu, J.; Frechet, J. M. J.; Toney, M. F. Dependence of Regioregular Poly(3-Hexylthiophene) Film Morphology and Field-Effect Mobility on Molecular Weight. *Macromolecules* **2005**, *38*, 3312–3319.
7. Meijer, E.; Detcheverry, C.; Baesjou, P.; Van Veenendaal, E.; de Leeuw, D.; Klapwijk, T. Dopant Density Determination in Disordered Organic Field-Effect Transistors. *J. Appl. Phys.* **2003**, *93*, 4831–4835.
8. Sirringhaus, H.; Wilson, R.; Friend, R.; Inbasekaran, M.; Wu, W.; Woo, E.; Grell, M.; Bradley, D. Mobility Enhancement in Conjugated Polymer Field-Effect Transistors through Chain Alignment in a Liquid-Crystalline Phase. *Appl. Phys. Lett.* **2000**, *77*, 406–408.
9. Erb, T.; Raleva, S.; Zhokhavets, U.; Gobsch, G.; Stühn, B.; Spode, M.; Ambacher, O. Structural and Optical Properties of Both Pure Poly(3-Octylthiophene)(P3OT) and P3OT/Fullerene Films. *Thin Solid Films* **2004**, *450*, 97–100.
10. DeLongchamp, D. M.; Vogel, B. M.; Jung, Y.; Gurau, M. C.; Richter, C. A.; Kirillov, O. A.; Obrzut, J.; Fischer, D. A.; Sambasivan, S.; Richter, L. J. Variations in Semiconducting Polymer Microstructure and Hole Mobility with Spin-Coating Speed. *Chem. Mater.* **2005**, *17*, 5610–5612.
11. Yang, H.; Shin, T. J.; Yang, L.; Cho, K.; Ryu, C. Y.; Bao, Z. Effect of Mesoscale Crystalline Structure on the Field-Effect Mobility of Regioregular Poly(3-Hexyl Thiophene) in Thin-Film Transistors. *Adv. Funct. Mater.* **2005**, *15*, 671–676.
12. Verploegen, E.; Mondal, R.; Bettinger, C. J.; Sok, S.; Toney, M. F.; Bao, Z. Effects of Thermal Annealing Upon the Morphology of Polymer−Fullerene Blends. *Adv. Funct. Mater.* **2010**, *20*, 3519–3529.
13. Smilgies, D. M. Scherrer Grain-Size Analysis Adapted to Grazing-Incidence Scattering with Area Detectors. *J. Appl. Crystallogr.* **2009**, *42*, 1030–1034.
14. Hlaing, H.; Lu, X.; Hofmann, T.; Yager, K.; Black, C.; Ocko, B. Nanoimprint-Induced Molecular Orientation in Semiconducting Polymer Nanostructures. *ACS Nano* **2011**, *5*, 7532–7538.
15. Kushida, T.; Nagase, T.; Naito, H. Air-Mediated Self-Organization of Polymer Semiconductors for High-Performance Solution-Processable Organic Transistors. *Appl. Phys. Lett.* **2011**, *98*, 063304-3.
16. Johnston, D. A.; Yager, K. G.; Nam, C. Y.; Ocko, B. M.; Black, C. T. One-Volt Operation of High-Current Vertical Channel Polymer Semiconductor Field-Effect Transistors. *Nano Lett.* **2012**, *8*, 4181–4186.
17. Aryal, M.; Trivedi, K.; Hu, W. W. Nano-Confinement Induced Chain Alignment in Ordered P3HT Nanostructures Defined by Nanoimprint Lithography. *ACS Nano* **2009**, *3*, 3085–3090.
18. Yang, Y.; Mielczarek, K.; Aryal, M.; Zakhidov, A.; Hu, W. Nanoimprinted Polymer Solar Cell. *ACS Nano* **2012**, *6*, 2877–2892.
19. Coakley, K.; Srinivasan, B.; Ziebarth, J.; Goh, C.; Liu, Y.; McGehee, M. Enhanced Hole Mobility in Regioregular Polythiophene Infiltrated in Straight Nanopores. *Adv. Funct. Mater.* **2005**, *15*, 1927–1932.
20. Allen, J. E.; Yager, K. G.; Hlaing, H.; Nam, C.-Y.; Ocko, B. M.; Black, C. T. Enhanced Charge Collection in Confined Bulk Heterojunction Organic Solar Cells. *Appl. Phys. Lett.* **2011**, *99*, 163301–163304.
21. Allen, J. E.; Yager, K. G.; Hlaing, H.; Nam, C. Y.; Ocko, B. M.; Black, C. T. Implementing Nanometer-Scale Confinement in Organic Semiconductor Bulk Heterojunction Solar Cells. *J. Photonics Energy* **2012**, *2*, 0210081–0210089.
22. Scavia, G.; Porzio, W.; Destri, S.; Barba, L.; Arrighetti, G.; Milita, S.; Fumagalli, L.; Natali, D.; Sampietro, M. Effect of the Silanization and Annealing on the Morphology of Thin Poly(3-Hexylthiophene) (P3HT) Layer on Silicon Oxide. *Surf. Sci.* **2008**, *602*, 3106–3115.
23. Xiao, X.; Hu, Z.; Wang, Z.; He, T. Study on the Single Crystals of Poly(3-Octylthiophene) Induced by Solvent-Vapor Annealing. *J. Phys. Chem. B* **2009**, *113*, 14604–14610.
24. Singh, C. R.; Gupta, G.; Lohwasser, R.; Engmann, S.; Balko, J.; Thelakkat, M.; Thurn-Albrecht, T.; Hoppe, H. Correlation of Charge Transport with Structural Order in Highly Ordered Melt-Crystallized Poly(3-Hexylthiophene) Thin Films. *J. Polym. Sci., Part B: Polym. Phys.* **2013**, *51*, 943–951.
25. Baker, J. L.; Jimison, L. H.; Mannsfeld, S.; Volkman, S.; Yin, S.; Subramanian, V.; Salleo, A.; Alivisatos, A. P.; Toney, M. F. Quantification of Thin Film Crystallographic Orientation Using X-Ray Diffraction with an Area Detector. *Langmuir* **2010**, *26*, 9146–9151.